EPI International Journal of Engineering
Volume 4, Number 2, August 2021, pp. 196-203
DOI: 10.25042/epi-ije.082021.12

*p*ISSN 2615-5109
*e*ISSN 2621-0541

Free Vibration Characteristics of Thin Spherical Shells

Koji Sekine [a,*]

[a]Field of Mechanical Engineering, Department of Creative Engineering, National Institute of Technology, Kushiro College.
Email:sekine@kushiro-ct.ac.jp

Abstract

Free vibration characteristics of thin spherical shells having freely boundary conditions are analyzed. In this study, the fundamental properties of natural vibration for the spherical shells are investigated. The power function is employed as the admissible function, displacement functions satisfying the geometric boundary conditions are expressed in the form of single series. The eigenvalue problem for free vibration of the shells derived by using the Lagrange's equation of motion, is processed numerically to acquire the natural frequencies and mode shapes. The reliability and accuracy of the present results are verified by convergence tendencies of the present solutions and comparisons of the data between the current analysis, FEM (finite element method) and published literatures. In numerical results, the variations of natural vibration characteristics of the shells due to the circumferential wavenumber and various shell geometries are illustrated.

Keywords: Free vibration; vibration of structural element; solid of revolution; spherical shell

1. Introduction

Spherical shells have a very broad range of application in industrial products as a structural element on the fields of mechanical, aerospace and civil engineering. In structural design, it is particularly significant that the natural vibration characteristics of the shells are comprehended as a valuable countermeasure against the resonance phenomenon.

Consequently, free vibration of the spherical shells has been widely and actively studied until recently. Niordson [1] presented the complete solution for axisymmetric and non-axisymmetric vibration of thin elastic spherical shell with two boundaries. Tornabene and Viola [2] dealt with the dynamical behaviour of hemispherical domes and spherical shell panels by using Generalized Differential Quadrature (GDQ) method. Lee [3] investigated the axisymmetric and asymmetric free vibration analysis of spherical caps, which have displacements and the rotations expressed by Chebyshev polynomials. Qu et al. [4] indicated a general formulation for vibration analyses of functionally graded shells of revolution subjected to arbitrary boundary conditions. Shi et al. [5] treated the free vibration analysis of open and closed shells with arbitrary boundary conditions. Xie et al. [6] presented an approach to analyze free vibrations of thin spherical shells with arbitrary boundary conditions and non-uniform thickness. Li et al. [7] described the free vibration of uniform and stepped annular-spherical shells with general boundary conditions by using a semi-analytical approach. Du et al. [8] showed the free vibration of spherical caps with uniform and stepped thickness subjected to various boundary conditions. Hu et al. [9] mentioned the free vibration characteristics of moderately thick annular spherical shell structure with general boundary conditions. In addition, Du et al. [10] proposed the free vibration characteristic of truncated spherical shell subjected to classical and elastic edge constraints. In the study introduced avobe, the governing equation of motion (the partial differential equations) is analyzed, and Chebyshev, Legendre and Jacobi polynomials are employed as the displacement admissible functions. Also, the analysis using artificial springs to give elastic boundary conditions has been solved by the Ritz method. On the other hand, the spherical shells deeper than the hemispherical shell and the sphere are rarely found, and there are few examples of variations in the natural vibration characteristics by the difference of the shell geometries.

Therefore, in this paper, the free vibration characteristics of the spherical shells is analyzed by using energy method and a commercial FEM (finite element method) software, SolidWorks simulation. Specifically, the power function is applied as the admissible function, and the energy functional of the shells consisting of the elastic strain energy and the kinetic energy are established. Furthermore, the eigenvalue problem for free vibration of the shells is derived by using the Lagrange's equation of motion. In numerical results, the

*Corresponding author. Tel.: +81-154-57-7294
Otanoshike-Nishi 2-32-1, Kushiro, Hokkaido
Japan, 084-0916

reliability and accuracy of the present solutions are showed from the point of view of the convergence for solutions and the comparisons with the data from published literatures and FEM software. Moreover, the variations of natural vibration characteristics such as natural frequencies and vibration modes of the shells by various shell geometries and the circumferential wavenumber are discussed.

2. Theory and Formulation

2.1. Geometry and displacement field of the spherical shell

The geometry and the coordinate system of the spherical shell are shown in Fig. 1. The coordinate system o-φ-θ-z is taken and the displacements in φ, θ and z directions at arbitrary points on the shell are represented by $\hat{u}$, $\hat{v}$ and $\hat{w}$, respectively. The shell has the hole at upper and lower poles, and the radius and thickness of the shell are denoted by R and h. Also, open angles at the poles are indicated by Φ_1 and Φ_2. As shown in Fig. 2, the shell has four types of geometry: with open angle Φ_2, with open angles Φ_1 and Φ_2 (symmetric or asymmetric to the equator) and sphere.

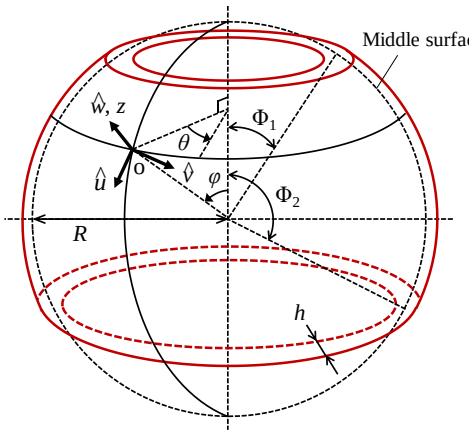

Figure 1. Geometry and the coordinate system of a spherical shell

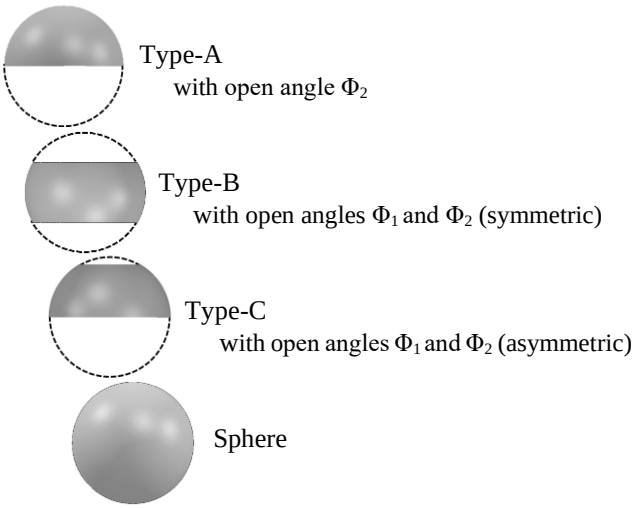

Figure 2. Geometry types of the spherical shell

On the bending deformation of the shell, the hypothesis of Kirchhoff-Love (Line elements perpendicular to the middle surface of the shell remain straight and perpendicular to the middle surface during deformation) is applied. Therefore, the displacements $\hat{u}$, $\hat{v}$ and $\hat{w}$ at arbitrary points of the shell can be written in Eq. (1). In this equation, u, v and w are the displacements on the middle surface of the shell and "t" denotes the time.

$$\begin{aligned}\hat{u}(\varphi,\theta,z,t)&=\left(1+\frac{z}{R}\right)u(\varphi,\theta,t)-\frac{z}{R}\frac{\partial w(\varphi,\theta,t)}{\partial\varphi}\\ \hat{v}(\varphi,\theta,z,t)&=\left(1+\frac{z}{R}\right)v(\varphi,\theta,t)-\frac{z}{R\sin\varphi}\frac{\partial w(\varphi,\theta,t)}{\partial\theta}\\ \hat{w}(\varphi,\theta,z,t)&=w(\varphi,\theta,t)\end{aligned} \tag{1}$$

2.2. Elastic strain and kinetic energies

Considering that the spherical shell consists of a linear elastic body, the strain-displacement relations are expressed as Eq. (2).

$$\begin{aligned}\varepsilon_\varphi&=\frac{1}{R}\left(\frac{\partial\hat{u}}{\partial\varphi}+\hat{w}\right)\\ \varepsilon_\theta&=\frac{1}{R}\left(\frac{1}{\sin\varphi}\frac{\partial\hat{v}}{\partial\theta}+\frac{\hat{u}}{\tan\varphi}+\hat{w}\right)\\ \gamma_{\varphi\theta}&=\frac{1}{R}\left(\frac{\partial\hat{v}}{\partial\varphi}+\frac{1}{\sin\varphi}\frac{\partial\hat{u}}{\partial\theta}-\frac{\hat{v}}{\tan\varphi}\right)\end{aligned} \tag{2}$$

Also, the stress-strain relations are expressed as Eq. (3). In this equation, Q_{ij} (i, j =1, 2, 6) are the stiffness coefficients composed of Young's modulus E and Poisson's ratio ν, respectively.

$$\begin{Bmatrix}\sigma_\varphi\\ \sigma_\theta\\ \tau_{\varphi\theta}\end{Bmatrix}=\begin{bmatrix}Q_{11}&Q_{12}&0\\ Q_{12}&Q_{22}&0\\ 0&0&Q_{66}\end{bmatrix}\begin{Bmatrix}\varepsilon_\varphi\\ \varepsilon_\theta\\ \gamma_{\varphi\theta}\end{Bmatrix}$$
$$Q_{11}=Q_{22}=\frac{E}{1-\nu^2},\ Q_{12}=\frac{\nu E}{1-\nu^2},\ Q_{66}=\frac{E}{2(1+\nu)} \tag{3}$$

Applying the elasticity theory, the elastic strain energy U stored in the shell due to elastic deformation is expressed by Eq. (4). In this equation, $[A]$ and $[D]$ are stretching and bending stiffness matrix, $\{\varepsilon\}$ and $\{\kappa\}$ are strain and curvature vectors on the middle surface of the shell. Also, the components of the matrices and the vectors are written by Eqs. (5) and (6).

$$\begin{aligned}U&=\frac{R^2}{2}\int_{-\frac{h}{2}}^{\frac{h}{2}}\int_0^{2\pi}\int_{\Phi_1}^{\Phi_2}(\sigma_\varphi\varepsilon_\varphi+\sigma_\theta\varepsilon_\theta+\tau_{\varphi\theta}\gamma_{\varphi\theta})\sin\varphi\,d\varphi\,d\theta\,dz\\ &=\frac{R^2}{2}\int_0^{2\pi}\int_{\Phi_1}^{\Phi_2}\left[\{\varepsilon\}^{\mathrm{T}}[A]\{\varepsilon\}+\{\kappa\}^{\mathrm{T}}[D]\{\kappa\}\right]\sin\varphi\,d\varphi d\theta\end{aligned} \tag{4}$$

$$[A]=\begin{bmatrix} A_{11} & A_{12} & 0 \\ A_{12} & A_{22} & 0 \\ 0 & 0 & A_{66} \end{bmatrix}, \quad [D]=\begin{bmatrix} D_{11} & D_{12} & 0 \\ D_{12} & D_{22} & 0 \\ 0 & 0 & D_{66} \end{bmatrix}$$

$$A_{ij}=hQ_{ij}\ ,\ D_{ij}=\frac{h^3}{12}Q_{ij}\ \ (i,\ j=1,2,6) \tag{5}$$

From now on, p_s and p_{rs} ($p\rightarrow u, v, w$ and $r, s\rightarrow \varphi, \theta$) denote the differentiation for $\partial p/\partial s$ and $\partial^2 p/\partial r\partial s$.

$$\{\varepsilon\}=\frac{1}{R}\left\{u_\varphi+w,\ \frac{u}{\tan\varphi}+\frac{v_\theta}{\sin\varphi}+w,\ v_\varphi-\frac{v}{\tan\varphi}+\frac{u_\theta}{\sin\varphi}\right\}^{\mathrm{T}}$$

$$\{\kappa\}=\frac{1}{R^2}\left\{u_\varphi-w_{\varphi\varphi},\ \frac{v_\theta}{\sin\varphi}-\frac{w_{\theta\theta}}{\sin^2\varphi}+\frac{u}{\tan\varphi}-\frac{w_\varphi}{\tan\varphi},\right.$$
$$\left. v_\varphi-\frac{v}{\tan\varphi}-\frac{2w_{\varphi\theta}}{\sin\varphi}+\frac{\cos\varphi\, w_\theta}{\sin^2\varphi}+\frac{u_\theta}{\sin\varphi}\right\}^{\mathrm{T}} \tag{6}$$

On the other hand, the kinetic energy T of the shell is evaluated by Eq. (7), where ρ is corresponding to the mass density of the material per unit volume.

$$T=\frac{R^2\rho}{2}\int_{-\frac{h}{2}}^{\frac{h}{2}}\int_0^{2\pi}\int_{\Phi_1}^{\Phi_2}\left\{\left(\frac{d\hat{u}}{dt}\right)^2+\left(\frac{d\hat{v}}{dt}\right)^2+\left(\frac{d\hat{w}}{dt}\right)^2\right\}\sin\varphi\, d\varphi d\theta dz$$
$$=\frac{R^2}{2}\int_0^{2\pi}\int_{\Phi_1}^{\Phi_2}\Big[I_{\mathrm{t}}(\dot{u}^2+\dot{v}^2+\dot{w}^2)+I_{\mathrm{r}}(\dot{u}^2+\dot{v}^2)$$
$$-2I_{\mathrm{r}}\left(\dot{u}\dot{w}_\varphi+\frac{\dot{v}\dot{w}_\theta}{\sin\varphi}\right)+I_{\mathrm{r}}\left(\dot{w}_\varphi^2+\frac{\dot{w}_\theta^2}{\sin^2\varphi}\right)\Big]\sin\varphi\, d\varphi d\theta \tag{7}$$

where the dot represents the derivative with respect to time, and the inertia terms can be written as follows:

$$I_{\mathrm{t}}=\rho h\ ,\quad I_{\mathrm{r}}=\frac{\rho h^3}{12R^2} \tag{8}$$

2.3. Derivation of the eigenvalue problem

Assuming that the shell maintains a harmonic vibrating at the angular frequency ω[rad/s], each displacement on the middle surface can be expressed as follows:

$$u(\varphi,\theta,t)=\sum_{i=0}^{I-1}u_i(t)\,X_{ui}(\varphi)Y_u(\theta)=\sin\omega t\sum_{i=0}^{I-1}U_i\,\varphi^i\cos N\theta$$
$$v(\varphi,\theta,t)=\sum_{i=0}^{I-1}v_i(t)\,X_{vi}(\varphi)Y_v(\theta)=\sin\omega t\sum_{i=0}^{I-1}V_i\,\varphi^i\sin N\theta \tag{9}$$
$$w(\varphi,\theta,t)=\sum_{i=0}^{I-1}w_i(t)\,X_{wi}(\varphi)Y_w(\theta)=\sin\omega t\sum_{i=0}^{I-1}W_i\,\varphi^i\cos N\theta$$

where N denotes the circumferential wave number, and the power function φ^i is employed as the admissible function $X_{pi}(\varphi)$ ($p\rightarrow u, v, w$) so that freely boundary conditions described in Eq. (10) are satisfied at the hole edges of the shell.

$$\text{Displacements}: \quad \hat{u}\big|_{\varphi=\Phi_{1,2}},\ \hat{v}\big|_{\varphi=\Phi_{1,2}},\ \hat{w}\big|_{\varphi=\Phi_{1,2}}\neq 0$$
$$\text{Slopes}: \quad \frac{\partial\hat{w}}{\partial\varphi}\bigg|_{\varphi=\Phi_{1,2}},\ \frac{\partial\hat{w}}{\partial\theta}\bigg|_{\varphi=\Phi_{1,2}}\neq 0 \tag{10}$$

Furthermore, the displacement functions given by Eq. (9) are substituted into the elastic strain and the kinetic energy described by Eqs. (4) and (7). Also, applying the Lagrangian ($L=T-U$) to the Lagrange's equation of motion written as Eq.(11), the generalized eigenvalue problem can be summed up by Eq. (12).

$$\frac{\partial}{\partial t}\left(\frac{\partial L}{\partial\dot{q}_i(t)}\right)-\frac{\partial L}{\partial q_i(t)}=0\quad (L=T-U) \tag{11}$$

where $q_i(t)$ ($q\rightarrow u, v, w$) are the generalized coordinates, which have been described in Eq. (9).

$$[K]\{a\}=\omega^2[M]\{a\}$$
$$\{a\}=\{U_i, V_i, W_i\}^{\mathrm{T}} \tag{12}$$

In Eq. (12), [K] and [M] represent the stiffness and the mass matrices, respectively. Natural frequencies ω and the corresponding eigenvectors $\{a\}$ are obtain by solving Eq. (12). Substituting the eigenvector $\{a\}$ including unknown coefficients U_i, V_i and W_i into the displacement functions given by Eq. (9), the natural vibration mode of the shells can be calculated. In numerical results, the natural frequencies ω are handled by the nondimensional frequency Ω expressed as follows:

$$\Omega=\omega R\sqrt{\frac{\rho}{E}} \tag{13}$$

3. Numerical Applications and Discussions

In this section, the accuracy and reliability of the present solutions are verified, and numerical study will be discussed on the free vibration characteristics of the spherical shells. In present numerical studies, Young's modulus E=190GPa, Poisson's ratio ν=0.3 and the volume density ρ=8000kg/m^3 are employed for the material constant of the spherical shells.

Within each tables and figures, the solutions by SolidWorks simulation as a commercial FEM (finite element method) software are indicated with present results. Also, in example results, m denotes mode number in the meridional direction.

Table 1 presents the convergence characteristics of nondimensional frequencies Ω with respect to variations of the number of terms I in displacement functions shown by Eq. (9). It is seen that nondimensional frequencies Ω converge with two or more significant figures, and the present solutions show good agreement with the results given by FEM simulation. Therefore, the number of terms I =10 is employed for *Type-A* and *Sphere*, and I =8 is applied to *Type-B* and *Type-C* in Eq. (9). In the case of *Type-A* and

Sphere, the shells have small open angles Φ_1 =0.01° and Φ_2 =179.99° due to avoid errors.

Table 2 demonstrates the comparisons of nondimensional frequency Ω of the spherical shell specified as *Type-A*. In the list, Niordson [1] shows the complete solution for natural vibration of the spherical shells, and Lee [3] presents the analytical solutions by using Chebyshev polynomials.

Table 3 shows the comparisons of nondimensional frequency Ω of the spherical shell specified as *Type-B*. Xie et al. [6] present an approach to analyze the free vibrations of thin spherical shells with various boundary conditions.

Table 4 gives the comparisons of nondimensional frequency Ω of the spherical shell specified as *Type-C*. Ref. [1] and [6] present the complete solution and an approach for the free vibration analysis of thin spherical shells, respectively.

Table 1. Convergence study of nondimensional frequencies Ω [*R*/*h*=100]

Φ_1 [deg]	Φ_2 [deg]	*N*	Num. of terms *I*	Mode No. *m* 1	2	3
0.01	90	0	7	0.8705	0.9530	0.9874
			8	0.8705	0.9526	0.9843
			9	0.8705	0.9525	0.9834
			10	0.8705	0.9525	0.9830
			FEM	0.8709	0.9528	0.9850
		7	7	0.2146	1.011	1.079
			8	0.2104	1.011	1.062
			9	0.2081	1.010	1.058
			10	0.2074	1.010	1.054
			FEM	0.2069	1.010	1.053
0.01	179.99	0	7	0.7349	0.8712	0.9527
			8	0.7349	0.8710	0.9265
			9	0.7349	0.8705	0.9261
			10	0.7349	0.8705	0.9246
			FEM	0.7360	0.8709	0.9245
		7	7	0.9908	1.048	1.188
			8	0.9884	1.019	1.151
			9	0.9873	1.011	1.063
			10	0.9867	1.006	1.046
			FEM	0.9858	1.002	1.019
30	90	0	5	0.9200	0.9824	1.018
			6	0.9197	0.9809	1.007
			7	0.9195	0.9796	1.002
			8	0.9195	0.9793	1.001
			FEM	0.9184	0.9792	1.002
		7	5	0.2253	0.6846	1.014
			6	0.2122	0.6664	1.013
			7	0.2088	0.6567	1.012
			8	0.2075	0.6510	1.012
			FEM	0.2067	0.6657	1.012

Table 2. Comparisons of nondimensional frequencies Ω [*R*/*h*=100, *Type-A*]

Φ_2 [deg]	*N*	*m*	Present	FEM	Ref. [1]	Ref. [3]
90	0	1	0.8705	0.8709	0.8705	0.8707
		2	0.9525	0.9528	-	0.9531
	2	1	0.0138	0.0130	0.0129	0.0138
		2	0.9174	0.9188	0.9174	0.9174
150	0	1	0.7648	0.7665	0.7648	-
	2	1	0.0429	0.0484	0.0461	-
		2	0.7916	0.7934	0.7917	-

Table 3. Comparisons of nondimensional frequencies Ω [*R*/*h*=100, *N*=2, *Type-B*]

Φ_1 [deg]	Φ_2 [deg]	*m*	Present	FEM	Ref. [1]	Ref. [6]
30	150	1	0.0408	0.0435	0.0432	0.0421
		2	0.0464	0.0500	0.0495	-
45	135	1	0.0189	0.0203	0.0201	0.0196
		2	0.0250	0.0268	0.0265	-
60	120	1	0.0122	0.0128	0.0127	0.0124
		2	0.0196	0.0206	0.0204	-

Table 4. Comparisons of nondimensional frequencies Ω [*R*/*h*=100, *N*=2, *Type-C*]

Φ_1 [deg]	Φ_2 [deg]	*m*	Present	FEM	Ref. [1]	Ref. [6]
30	90	1	0.0133	0.0126	0.0126	0.0123
		2	0.0471	0.0515	0.0510	-
	120	1	0.0149	0.0155	0.0153	0.0151
		2	0.0445	0.0492	0.0478	-
60	90	1	0.0104	0.0104	0.0103	0.0100
		2	0.0223	0.0230	0.0226	-

In Tables 2−4, it's observed that the present solutions agree well with the ones obtained by the commercial FEM software and the references. As can be seen, the accuracy, validity and the verification of the present solutions can be confirmed in the view point of these comparisons. In the following, the present and FEM solutions are illustrated with respect to the shell geometries of *Type-A*, *B* and *C*.

Fig. 3 shows the variations of the nondimensional frequency Ω with respect to the circumferential wave number *N* for the spherical shell specified as *Type-A*. In the figure, the solid and broken lines indicate the present solutions, and the small circles show FEM solutions. For any of the open angle Φ_2, the fundamental frequency has been obtained at *N*=1, and so a significantly low frequency can be illustrated because the spherical shells behave like a rigid body motion at *N*=1. At axisymmetric mode with *N*=0, the nondimensional frequency of *Sphere* is the lowest, and at

Φ_2=30°(shallow cap), high nondimensional frequency can be achieved. Whereas, when *N* is larger than 1, the hemispherical shell(dome) with Φ_2=90° has the lowest nondimensional frequency, and the shell geometry of *Sphere* gives high one.

Fig. 4 gives the variations of the nondimensional frequency Ω with respect to the open angle Φ_2 for the spherical shell characterized as *Type-A*. In this figure, the lowest nondimensional frequency is given at Φ_2 =90° for each *N* except *N*=0, and it is effective to set the open angle Φ_2 greater than 150° in order to increase the natural frequency of the shells.

Fig. 5 shows the vibration modes with respect to the open angle Φ_2 for the spherical shell specified as *Type-A*. In the figure, nondimensional frequency Ω and Ω_{FEM} by the present and FEM solution are indicated under each vibration modes. At *N*=0, the axisymmetric mode shapes are illustrated for each open angle Φ_2 , and the node exists on the circumferential direction for the meridional direction mode number *m*=2. On the other hand, *N*=7 as the non-axisymmetric mode, it's recognized that multiple waves appear at the circumferential direction of the shell. Also, the waves exist clearly at the hole edge except *Sphere*.

Fig. 6 shows the variations of the nondimensional frequency Ω with respect to the circumferential wave number *N* for the spherical shell specified as *Type-B*. In this figure, the lines and the small circles indicate the present solutions and FEM ones, respectively. For any of the open angle Φ_1 , the fundamental frequency has been given at *N*=1.

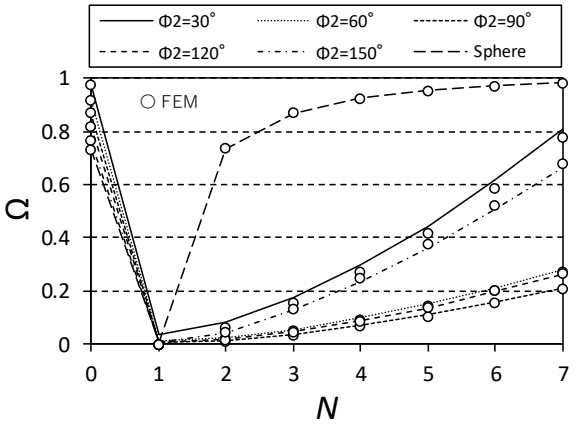

Figure 3. Variations of nondimensional frequencies Ω versus the circumferential wave number *N*
[*R*/*h*=100, *m*=1, *Type-A*]

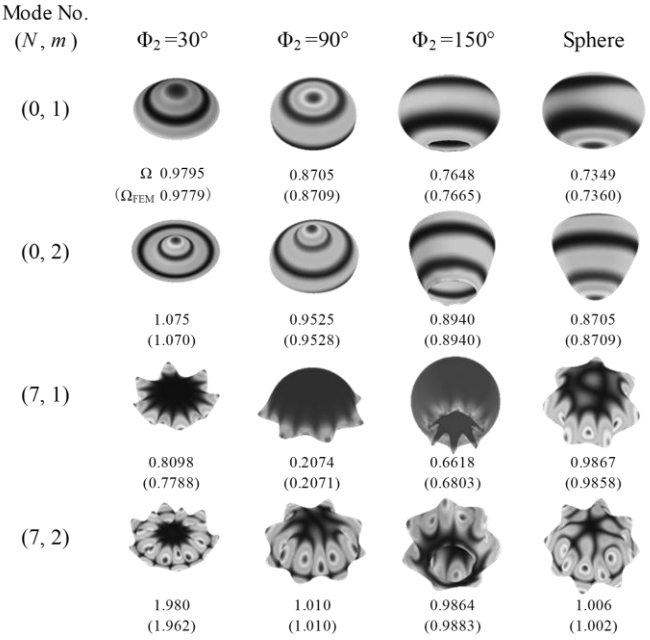

Figure 5. Vibration modes of the spherical shells
[*R*/*h*=100, *Type-A*]

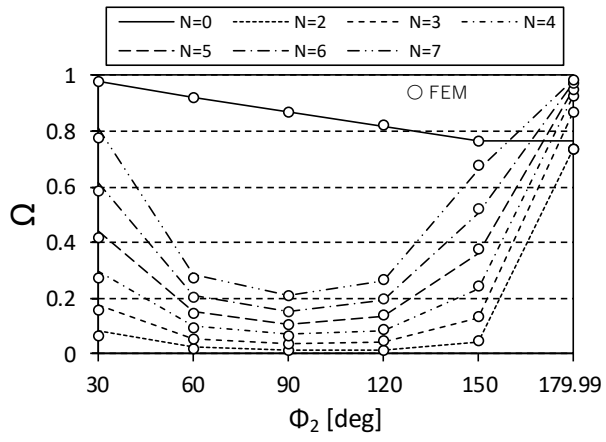

Figure 4. Variations of nondimensional frequencies Ω versus the open angle Φ_2
[*R*/*h*=100, *m*=1, *Type-A*]

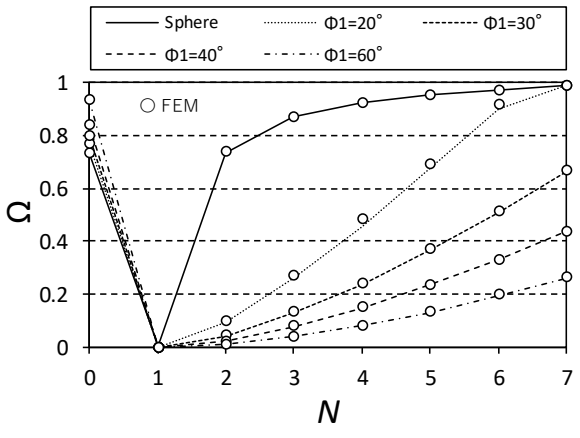

Figure 6. Variations of nondimensional frequencies Ω versus the circumferential wave number *N*
[*R*/*h*=100, *m*=1, Φ_2 =180°−Φ_1 , *Type-B*]

For N=0 as an axisymmetric mode, it turns out that the nondimensional frequency of *Sphere* is the lowest, and high nondimensional frequency can be obtained at Φ_1=60°. When N is larger than 1, the opposite tendency can be seen. That is, the shell geometry of *Type-B* with Φ_1=60° gives the lowest nondimensional frequency, and *Sphere* shows high one.

Fig. 7 gives the variations of the nondimensional frequency Ω with respect to the open angle Φ_1 for the spherical shell characterized as *Type-B*. In the figure, the lowest nondimensional frequency is given at Φ_1 =60° for each N except N=0. If the design of a high natural frequency for the shells is required, it's desirable to set the open angle Φ_1 less than 10°.

Fig. 8 shows the vibration modes with respect to the open angle Φ_1 for the spherical shell specified as *Type-B*. As Φ_1 increases, the geometry of the shell becomes closer to a ring. At N=0 as an axisymmetric vibration, mode shapes of the torus type are indicated for each open angle Φ_1. Also, it is seen that according as the circumferential wave number N becomes larger, the waves increase on the circumferential direction of the shells. In addition, a vertically symmetrical vibration modes appear except for N=7 with Φ_1=30°.

Fig. 9(a)-(c) show the variations of the nondimensional frequency Ω versus the circumferential wave number N for the spherical shell characterized as *Type-C* having the open angle Φ_1 =10°, 30° and 60°, respectively. Where, the lines and the small circles denote the present and FEM solutions. As shown in these figures, when N is larger than 1, the shells having Φ_2 =90° give the lowest nondimensional frequency for each the open angle Φ_1. Also, for the shells with the open angles Φ_2 =60°, 90° and 120°, it can be seen that the nondimensional frequencies are hardly affected by the change of the open angles Φ_1. Furthermore, Fig.9(a) presents that the shallow shells with Φ_2 =30° or the deep shells with Φ_2 =150° give high nondimensional frequency while in N larger than 1.

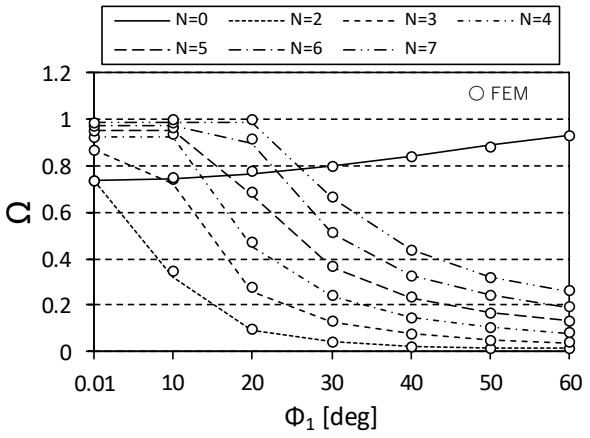

Figure 7. Variations of nondimensional frequencies Ω versus the open angle Φ_1
[R/h=100, m=1, Φ_2 =180°−Φ_1 , *Type-B*]

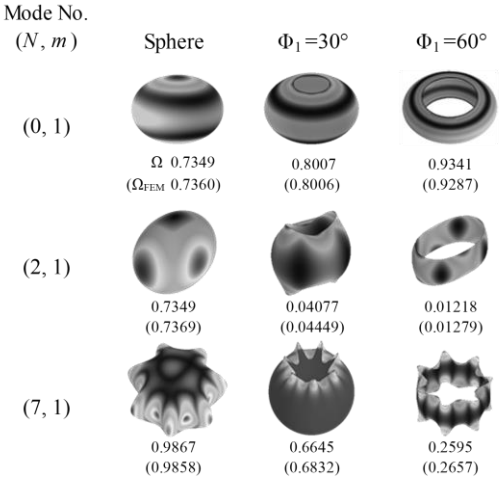

Figure 8. Vibration modes of the spherical shells
[R/h=100, *Type-B*]

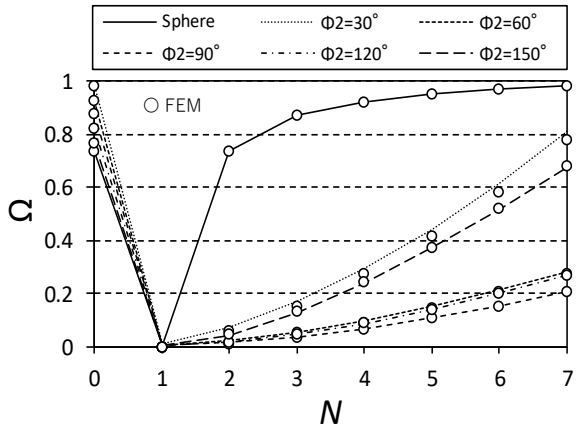

Figure 9(a). Variations of nondimensional frequencies Ω versus the circumferential wave number N
[R/h=100, m=1, Φ_1 =10°, *Type-C*]

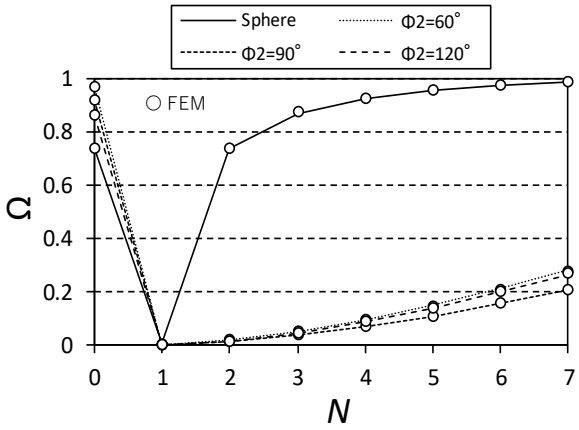

Figure 9(b). Variations of nondimensional frequencies Ω versus the circumferential wave number N
[R/h=100, m=1, Φ_1 =30°, *Type-C*]

Fig. 10(a), (b) give the variations of the nondimensional frequency Ω versus the open angle Φ_2 for the spherical shell specified as *Type-C* having the open angle Φ_1 =10°, 30° and 60°, respectively.

In these figures, for each open angles Φ_1, the lowest nondimesional frequency can be obtained by the shells with Φ_2 =90°. When high natural frequency of the shells is required in the structural design due to avoid the resonance, it is effective to adapt the shells to be shallow(Φ_2 =30°) or deep(Φ_2 =150°). Also, when Φ_2 increase as the shells becomes deep, the nondimensional frequency decreases linearly for *N*=0 as an axisymmetric mode.

Fig. 11 indicates the vibration modes with respect to the open angles Φ_1 and Φ_2 for the spherical shell specified as *Type-C*. It is worth noting that the influences on the nondimensional frequency due to the changes in Φ_1 are weak for each the open angle Φ_2. In particular, when the circumferential wave number *N*=7, the mode shapes indicate local wavy deformations at lower hole edge. Therefore, the effects due to the changes of Φ_1 on the nondimensional frequencies are very small, and the nondimensional ones decrease slightly. On the contrary, when *N*=0, it is recognized that nondimensional ones increase as Φ_1 increase.

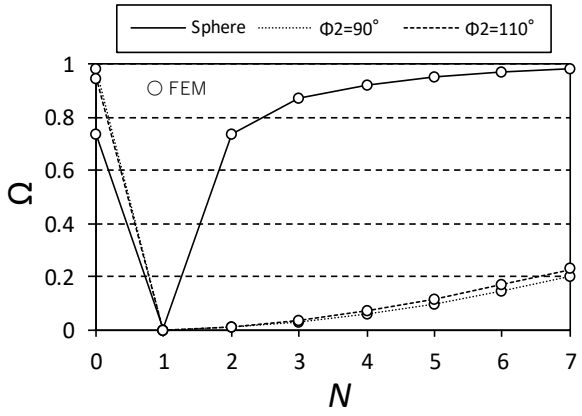

Figure 9(c). Variations of nondimensional frequencies Ω versus the circumferential wave number *N*
[*R*/*h*=100, *m*=1, Φ_1 =60°, *Type-C*]

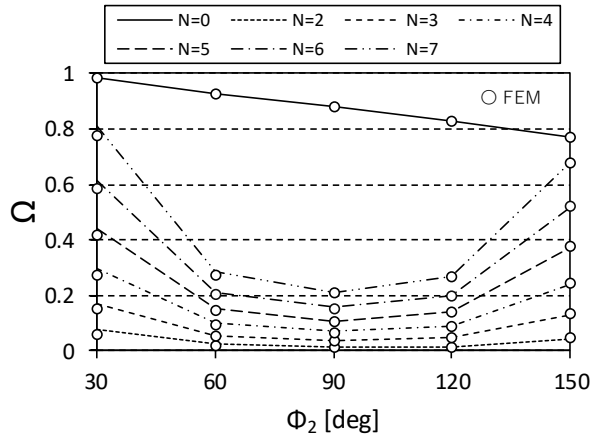

Figure 10(a). Variations of nondimensional frequencies Ω versus the open angle Φ_2
[*R*/*h*=100, *m*=1, Φ_1 =10°, *Type-C*]

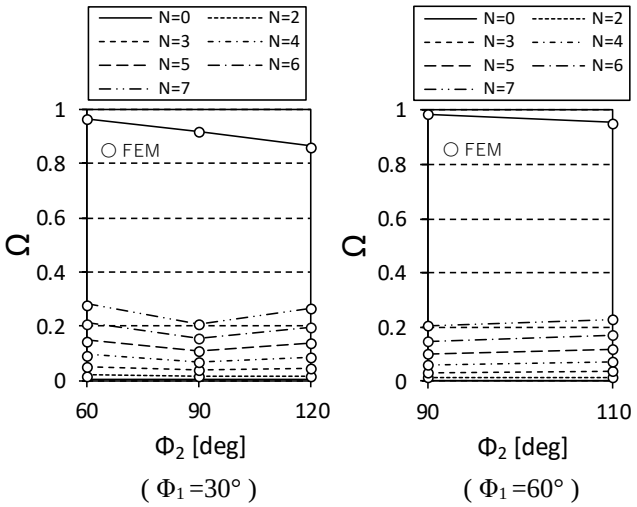

Figure 10(b). Variations of nondimensional frequencies Ω versus the open angle Φ_2 [*R*/*h*=100, *m*=1, *Type-C*]

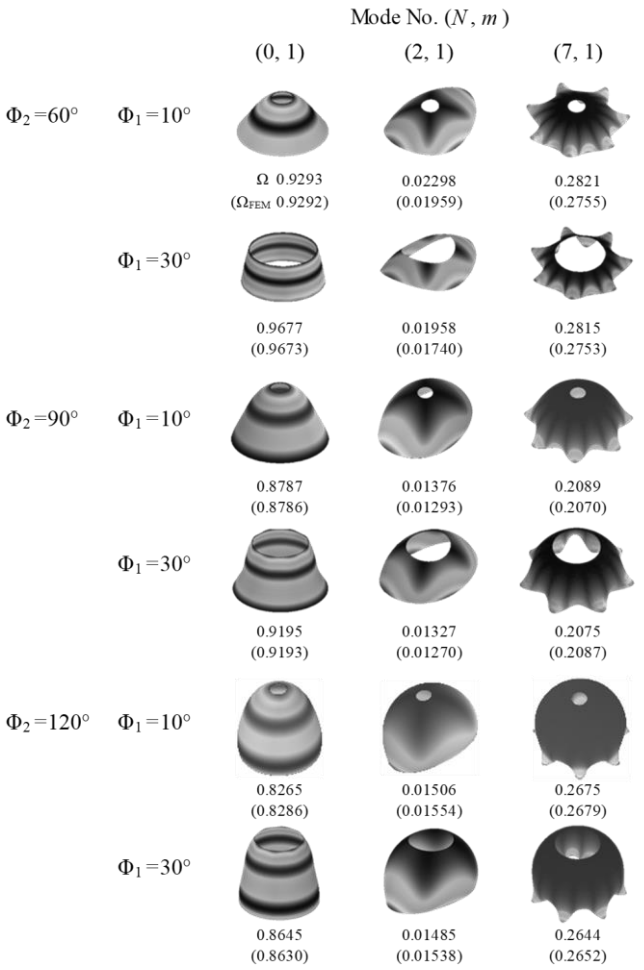

Figure 11. Vibration modes of the spherical shells
[*R*/*h*=100, *Type-C*]

4. Conclusions

This paper has dealt with the free vibration characteristics of thin spherical shells having freely boundary conditions.

First of all, the formulation of natural vibration analysis of the spherical shell has been expanded by applying the energy method. Also, the convergence study of the present solutions with respect to the number of terms in displacement functions has been indicated. Furthermore, the accuracy, validity and the verification of the present solutions have been confirmed through the comparisons with the solutions given by the commercial FEM software and the references.

In several numerical example, the present and FEM solutions for the free vibration characteristics of the shells have been illustrated with respect to the shell geometries specified by *Type-A*, *B* and *C*. Practically, the variations of natural frequencies and vibration modes of the shells due to the circumferential wavenumber, various shell geometries and the open angles have been illustrated in the figures.

It is expected that the present solution obtained in this study be able to suggest the fundamental properties of the spherical shells. Also, the present solution will give a reference data in similar studies of the solids of revolution. In addition, taking into account the problem due to avoid the resonance of the structures, the present results can be referred for the optimization design of the spherical shells.

References

[1] Niordson F I. Free vibrations of thin elastic spherical shells. Int J Solids Struct 1984;20(7):667-678.

[2] Tornabene F, Viola E. Vibration analysis of spherical structural elements using the GDQ method. Comput Math Appl 2007;53:1538-60.

[3] Lee J. Free vibration analysis of spherical caps by the pseudospectral method. J Mech Sci Technol 2009;23:221-8.

[4] Qu Y, Long X, Yuan G, Meng G. A unified formulation for vibration analysis of functionally graded shells of revolution with arbitrary boundary conditions. Compos B Eng 2013;50:381-402.

[5] Shi D, Zhao Y, Wang Q, Teng X, Pang F. A unified spectro-geometric-Ritz method for vibration analysis of open and closed shells with arbitrary boundary conditions. Shock Vib 2016; Article ID 4097123: 30pages.

[6] Xie K, Chen M, Li Z. A semi-analytical method for vibration analysis of thin spherical shells with elastic boundary conditions. J Vibroeng 2017;19(4):2312-30.

[7] Li H, Pang F, Chen H. A semi-analytical approach to analyze vibration characteristics of uniform and stepped annular-spherical shells with general boundary conditions. Europe J Mech / A Solids 2019;74:48–65.

[8] Du Y, Huo R, Pang F, Li S, Huang Y, Zhang H. Free vibration of spherical cap subjected to various boundary conditions. Adv Mech Eng 2019;11(9):1-12.

[9] Hu B, Gao C, Zhang H, Li H, Pang F, Lang J. Free vibration characteristics of moderately thick spherical shell with general boundary conditions based on Ritz method. Shock Vib 2020; Article ID 4130103:20pages.

[10] Du Y, Sun L, Li S, Li S. Vibration analysis of truncated spherical shells under various edge constraints. Thin-Walled Struct 2020;147:106544.